Textile Modeling with Beams and Contact: A Biaxial Tension Study

Celso Jaco Faccio Júnior[1], Alfredo Gay Neto[1], Peter Wriggers[2]

[1]*Polytechnic School, University of São Paulo*
Av. Prof. Almeida Prado, trav.2 nº. 83, 05508-900, São Paulo/SP, Brazil
celsojf@usp.br, alfredo.gay@usp.br
[2]*Institute of Continuum Mechanics, Leibniz Universität Hannover*
An der Universität 1, 30823, Garbsen, Germany
wriggers@ikm.uni-hannover.de

Abstract. The mechanical response of textile composite materials depends substantially on the configuration of fibers that compose a given textile material pattern. The fibers' configuration is, however, difficult to be predicted due to several factors such as their large deformability and nonlinear mechanical response. The large deformability of textiles results from the characteristics of these materials, in which the axial stiffness of yarns is predominant. The overall nonlinear response is a complex phenomenon that includes, but is not limited to, complex yarns' contact interactions. As a possibility to overcome these difficulties, in this work, the textile's mechanical behavior is modeled with beam elements and contact formulations. A geometrically-exact structural formulation that can handle large displacements and finite rotations is adopted for the beam elements. Moreover, two contact formulations including nonlinear compliance laws are employed. The former contact formulation considers surface-to-surface interaction while the latter uses a beam-to-beam smooth approach. This textile modeling strategy, including both contact formulations, is verified with biaxial tension experimental results. The advantages and disadvantages of each contact formulation when compared to the experimental results are discussed.

Keywords: Textile modeling, Biaxial tension, Contact, Beam

1 Introduction

The mechanical behavior of dry textiles is a topic of great complexity due to several factors, such as their nonlinear mechanical response, large deformability, and yarns' contact interaction. In this context, an example of experiment of great importance is the biaxial tension. In this experiment, a textile sample is attached to an apparatus where distinct displacements are imposed in each main direction, while reaction forces are simultaneously measured.

The objective of this work is to compare and discuss the mechanical behavior of a plain woven glass fabric under biaxial tension considering experimental results from [1], and a modeling strategy that combines a geometrically-exact beam theory with surface-to-surface [2] and beam-to-beam contact formulations [3].

2 Contact Formulations

In both here adopted surface-to-surface and beam-to-beam contact formulations the contact interaction is treated as pointwise. Pointwise interaction assumes that the contact phenomena can be described by resulting forces acting at a single point in each body. Therefore, a fundamental step is to obtain the locations, or material points, where these contact forces may take place. The problem of finding these material points is frequently named as "Closest Point Projection (CPP)" or "Local Contact Problem (LCP)" [4, 5]. Despite the nomenclature, the goal is to locate points where the contact interaction is likely to occur. Once these points are located, a LCP solution is found.

For a given LCP solution, it is possible to evaluate the distance (or gap) between these material points and ultimately verify their contact interaction. If contact is confirmed, contact forces take place at the material points

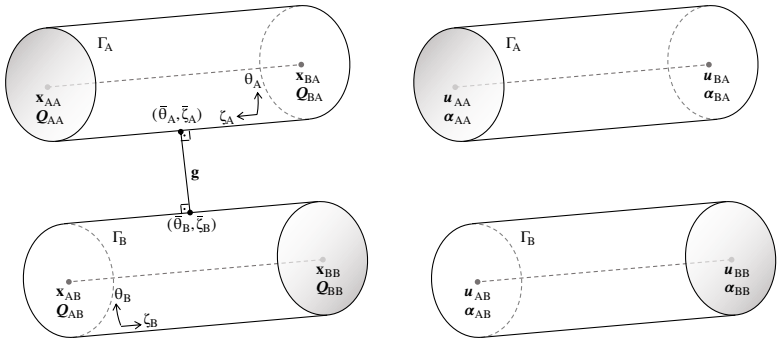

(a) Surfaces parametrizations and Local Contact Problem. Extracted from [2].

(b) Surfaces DOFs involved.

Figure 1. Surfaces Γ_A and Γ_B prone to contact.

previously obtained. These contact forces are calculated according to an interface law that may even be experimentally obtained. These contact forces limit and rule the surface's penetration, which is admitted and controled to some extent. This process occurs multiple times according to the model number of contact elements and deformation along time, which is considered in a numerical simulation. The surface-to-surface contact formulation is detailed in [6, 7] while the beam-to-beam contact formulation is presented in [3, 8]. The subsections below aim to provide an overview of both formulations to enhance overall comprehension.

2.1 Surface-to-Surface Contact Formulation

Consider two contact surfaces Γ_A and Γ_B, which are prone to contact. Figure 1a illustrates a LCP solution in which the material points are located in terms of the surfaces' convective coordinates as $\boldsymbol{c}_A = [\zeta_A \; \theta_A]^T$ in Γ_A and $\boldsymbol{c}_B = [\zeta_B \; \theta_B]^T$ in Γ_B. For convenience, these coordinates can be joined in a single vector $\boldsymbol{c}$ as

$$\boldsymbol{c} = \begin{bmatrix} \boldsymbol{c}_A & \boldsymbol{c}_B \end{bmatrix}^T = \begin{bmatrix} \zeta_A & \theta_A & \zeta_B & \theta_B \end{bmatrix}^T. \tag{1}$$

An important aspect of contact formulations are the degrees of freedom (DOFs) considered according to the structural model. In the surface-to-surface contact formulation, translational ($\boldsymbol{u}$) and rotational ($\boldsymbol{\alpha}$) degrees of freedom are treated. Figure 1b illustrates the degrees of freedom of Γ_A and Γ_B. Again, these generalized displacements can be joined into a single vector $\boldsymbol{d}$ given as

$$\boldsymbol{d} = \begin{bmatrix} \boldsymbol{d}_A & \boldsymbol{d}_B \end{bmatrix}^T = \begin{bmatrix} \boldsymbol{u}_{AA}^T & \boldsymbol{u}_{BA}^T & \boldsymbol{\alpha}_{AA}^T & \boldsymbol{\alpha}_{BA}^T & \boldsymbol{u}_{AB}^T & \boldsymbol{u}_{BB}^T & \boldsymbol{\alpha}_{AB}^T & \boldsymbol{\alpha}_{BB}^T \end{bmatrix}^T. \tag{2}$$

Considering then these parametrizations, Γ_A and Γ_B can be expressed as

$$\begin{aligned} \Gamma_A(\zeta_A, \theta_A) &= \hat{\boldsymbol{x}}(\zeta_A) + \hat{\boldsymbol{a}}(\zeta_A, \theta_A) \\ \Gamma_B(\zeta_B, \theta_B) &= \hat{\boldsymbol{x}}(\zeta_B) + \hat{\boldsymbol{a}}(\zeta_B, \theta_B) \end{aligned} \tag{3}$$

where $\hat{\boldsymbol{x}}(\zeta_i)$ with $i = A, B$ is a function to define the beam axis and $\hat{\boldsymbol{a}}(\zeta_i, \theta_i)$ with $i = A, B$ is a function to describe the beams' external lateral surface. In the adopted surface-to-surface contact formulation elliptical cross-sections are adopted. The contact surfaces' parametrization is detailed in [9].

Considering a pair of contact surfaces Γ_A and Γ_B, it is possible now to formulate a single gap function $\boldsymbol{g}$ including all their respective convective coordinates and degrees of freedom. The gap function $\boldsymbol{g}$ is defined as

$$\boldsymbol{g} = \hat{\boldsymbol{g}}(\boldsymbol{c}, \boldsymbol{d}) = \Gamma_A - \Gamma_B. \tag{4}$$

The gap function $\boldsymbol{g}$ spatially represents the difference (distance) between Γ_A and Γ_B. Therefore, the LCP can be expressed, for a given gap function $\boldsymbol{g}$, as

$$\boldsymbol{r} = \begin{bmatrix} \Gamma_{A,\zeta_A} \cdot \boldsymbol{g} \\ \Gamma_{A,\theta_A} \cdot \boldsymbol{g} \\ -\Gamma_{B,\zeta_B} \cdot \boldsymbol{g} \\ -\Gamma_{B,\theta_B} \cdot \boldsymbol{g} \end{bmatrix} = \boldsymbol{o}_4 \tag{5}$$

where the notation $A_{,b} = \partial A/\partial b$ is adopted to represent partial derivatives, and $\boldsymbol{o}_4$ is used to represent a null column matrix of order four. The solution of the LCP in equation eq. (5) is a set of four convective coordinates $\bar{\boldsymbol{c}} = [\bar{\boldsymbol{c}}_A \ \bar{\boldsymbol{c}}_B]^T = [\bar{\zeta}_A \ \bar{\theta}_A \ \bar{\zeta}_B \ \bar{\theta}_B]^T$. For an LCP solution $\bar{\boldsymbol{c}}$ it is still possible to obtain the contact forces direction and magnitude respectively from $\boldsymbol{g}$ and $g_n = \|\boldsymbol{g}\|$. Finally, the normal contact contribution to the model weak form can be calculated as

$$\delta W_c = \boldsymbol{f}_n \cdot \delta \boldsymbol{g} = f_n \delta g_n, \tag{6}$$

where $\boldsymbol{f}_n$ is the normal force contact vector that is obtained from a normal interface law, f_n is the normal force magnitude given by $f_n = \|\boldsymbol{f}_n\|$, and "$\delta$" is used to indicate virtual quantities. In the case of a linear interface law, a single linear coefficient ε is necessary to rule surfaces' penetration. This parameter is commonly named as a penalty parameter.

2.2 Beam-to-Beam Contact Formulation

Consider now two curves Γ_A and Γ_B as contact elements in a 3-dimensional space. In this case one can formulate the LCP as the closest point bilateral projection between these curves. Figure 2a illustrates a LCP solution between Γ_A and Γ_B. Moreover, it is possible to express the material point location in each curve using a single convective coordinate. Consider therefore two convective coordinates ξ_A and ξ_B that are respectively associated with Γ_A and Γ_B. The convective coordinates of Γ_A and Γ_B can be joined into a single vector $\boldsymbol{c}$ defined as

$$\boldsymbol{c} = \begin{bmatrix} \boldsymbol{c}_A & \boldsymbol{c}_B \end{bmatrix}^T = \begin{bmatrix} \xi_A & \xi_B \end{bmatrix}^T. \tag{7}$$

It is convenient now to introduce the DOFs associated with the beam-to-beam contact formulation. For the proposed formulation only translational ($\boldsymbol{u}$) DOFs are considered. Figure 2b illustrates the translational DOFs adopted for Γ_A. The translational DOFs of Γ_A and Γ_B can also be respectively joined into a single vector $\boldsymbol{d}$ defined as

$$\boldsymbol{d} = \begin{bmatrix} \boldsymbol{d}_A & \boldsymbol{d}_B \end{bmatrix}^T = \begin{bmatrix} \boldsymbol{u}_{AA}^T & \boldsymbol{u}_{BA}^T & \boldsymbol{u}_{CA}^T & \boldsymbol{u}_{AB}^T & \boldsymbol{u}_{BB}^T & \boldsymbol{u}_{CB}^T \end{bmatrix}^T. \tag{8}$$

In the proposed beam-to-beam contact formulation a spline description is adopted to describe the curves in space. A spline can be seen as an elegant way to describe curves in space with some desirable features. A spline curve is obtained by combining a set of points with special basis functions to guarantee a certain level of continuity [10]. For the proposed formulation, each spline segment is defined by a set of three points (nodes) and the basis functions are calculated to guarantee at least C^1 continuity. The process of constructing the spline elements is detailed for the adopted beam-to-beam contact in [3]. It is possible now to properly express the contact elements Γ_A and Γ_B as

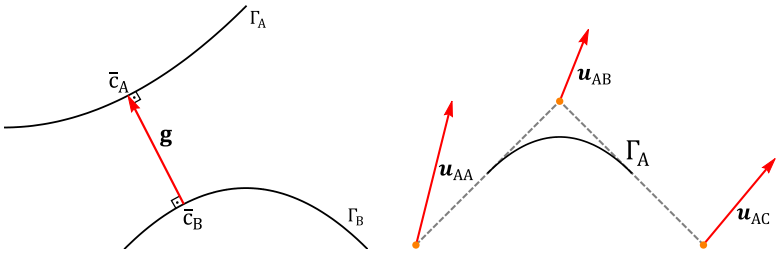

(a) Surfaces parametrizations and Local Contact Problem. Adapted from [3].

(b) Spline DOFs involved. Taken from [3].

Figure 2. Splines Γ_A and Γ_B prone to contact.

$$\begin{aligned} \Gamma_A(c_A, \boldsymbol{d}_A) &= \boldsymbol{C}_A(\xi_A) \\ \Gamma_B(c_B, \boldsymbol{d}_B) &= \boldsymbol{C}_B(\xi_B) \end{aligned} \tag{9}$$

where $\boldsymbol{C}_A(\xi_A)$ and $\boldsymbol{C}_B(\xi_B)$ are the corresponding spline curves. The gap function $\boldsymbol{g}$ can be then defined, considering two contact Γ_A and Γ_B, as

$$\boldsymbol{g} = \hat{\boldsymbol{g}}(\boldsymbol{c}, \boldsymbol{d}) = \Gamma_A - \Gamma_B. \tag{10}$$

The gap function $\boldsymbol{g}$ represents then the distance between curves Γ_A and Γ_B in space. The gap function is particularly important for the contact formulation since it gathers all convective coordinates and DOFs from Γ_A and Γ_B. For a given gap function $\boldsymbol{g}$ with curves the LCP is simply formulated as

$$\boldsymbol{r} = \begin{bmatrix} \Gamma_{A,\xi_A} \cdot \boldsymbol{g} \\ -\Gamma_{B,\xi_B} \cdot \boldsymbol{g} \end{bmatrix} = \boldsymbol{o}_2. \tag{11}$$

$\boldsymbol{o}_2$ indicates a null column matrix of order two. The solution of eq. (11) is a set of two convective coordinates $\bar{\boldsymbol{c}} = [\bar{\boldsymbol{c}}_A^T \; \bar{\boldsymbol{c}}_B^T]^T = [\bar{\xi}_A \; \bar{\xi}_B]$ corresponding to material points in Γ_A and Γ_B. A LCP solution is, however, not enough to ultimately characterize a contact interaction since until now only curves were considered. To characterize the contact interaction it is necessary to attach cross-sectional information to the curves. It is possible to conceive a contact surface by sweeping the spline curve with the cross-section defined. For the proposed formulation only circular cross-sections are adopted. Assuming that two radii r_A and r_B are respectively associated with Γ_A and Γ_B, it is feasible to evaluate the contact magnitude. The contact magnitude, or effective gap, is therefore calculated as

$$g_e = \hat{g}_e(\boldsymbol{c}, \boldsymbol{d}) = \|\Gamma_A - \Gamma_B\| - (r_A + r_B). \tag{12}$$

Finally, with all these quantities, the normal contact force contribution to the weak form can be obtained as

$$\delta W_c = \boldsymbol{f}_n \cdot \delta(g_e \boldsymbol{n}) \tag{13}$$

where $\boldsymbol{f}_n$ is the normal contact force vector, $\boldsymbol{n}$ is the normal contact direction given by $\boldsymbol{n} = \boldsymbol{g}/\|\boldsymbol{g}\|$, and the notation "$\delta$" is used to indicate virtual quantities. A broad range of interface laws (including nonlinear) can be adopted to calculate the normal contact forces. However, in a linear case, a single penalty parameter ε that is directly proportional to the penetration magnitude is necessary.

3 Structural Formulation

For both contact formulations presented a geometrically-exact beam theory is used. The geometrically-exact beam theory was introduced in the seminal works of Simo [11–13] and after expanded by many authors. A detailed description of the beam theory here adopted is presented in [14, 15]. To keep work conciseness only the kinematic of a material point for the beam theory is presented. In the geometrically-exact beam theory the position of a beam element generic point $\boldsymbol{x}$ is depicted as

$$\boldsymbol{x} = \zeta \boldsymbol{e}_3^r + \boldsymbol{u} + \boldsymbol{Q}\boldsymbol{a}^r, \tag{14}$$

where ζ is an beam axis convective coordinate, $\boldsymbol{e}_3^r$ is the beam axis direction in the reference configuration (straight beam), $\boldsymbol{u}$ is the beam axis displacement field, $\boldsymbol{Q}$ is a rotation tensor field, mapping the cross-section from the reference configuration to the current configuration, $\boldsymbol{a}^r$ is a vector reading the cross-section shape in the reference configuration. An important aspect of eq. (14) is that this generic point can experience arbitrary large displacements and finite rotations. Moreover, after some mathematical effort, it is possible to establish equilibrium by calculating all contributions to the weak form [15, 16].

4 Textile Modeling

To model the biaxial tension textile behavior the Giraffe finite element solver [17–19] is combined with the TexGen® [20] textile modeling tool. The Giraffe finite element solver is a compelling tool since it includes several contact formulations and geometrically-exact beam elements. Moreover, the TexGen® software is a powerful tool specialized in the geometric modeling of textiles.

To build the biaxial tension computational model, three steps are necessary. First, an originally developed software generates a Python script for the TexGen® including essential information such as the number of yarns in each direction, the in-plane yarn spacing, the out-of-plane yarn spacing (gap between yarn's), the yarn in-plane length. Second, the TexGen® software generates a file containing a detailed geometrical description of the yarns. And third, the originally developed software reads this information and generates a corresponding Giraffe input file.

5 Biaxial Tension Study

The objective of this study is to compare the experimental and computational modeling results with respect to the mechanical behavior of a plain glass fabric under biaxial tension. The experimental results here considered are presented in [1]. For the computational modeling, a geometrically-exact beam theory is combined with two distinct contact formulations, a surface-to-surface and a beam-to-beam spline-based contact formulation. The results concerning the biaxial tension modeling with the surface-to-surface are presented in [2].

The biaxial tension experiment is defined by simultaneous tension imposed at both main textile directions (warp and weft). During the experiment, force-strain graphics are obtained in each direction. Moreover, different strain levels can be imposed in each direction. The strain ratio of a biaxial tension experiment is defined as $k = \epsilon_{warp}/\epsilon_{weft}$, where "warp" and "weft" are assumed to be respectively the "x" and "y" directions.

To model the glass fabric a material with a tensile stiffness (EA) of $38000N$, a Poisson ratio of 0.2, and a specific mass of $2540kg/m^3$ is adopted. For the surface-to-surface contact formulation that takes ellipsoidal cross-sections a beam semi-major axis of $1.136364mm$ and a semi-minor axis of $0.2840909mm$ are considered. For the beam-to-beam contact formulation, a circular cross-section with a radius of $0.2840909mm$ is assumed. It is important to note that the circular cross-section is used only to model the contact interaction while the structural properties are kept the same in both models. To model the very low bending stiffness of the textile, a reduction factor of 10^{-1} is applied to the lower moment of inertia. In this example, all simulations are performed with six yarns in each direction, an in-plane length of $40.90909mm$, an in-plane spacing between yarns of $4.54545mm$, and an out-of-plane spacing between yarns surfaces of $0.11364mm$.

In all surface-to-surface simulations a penalty parameter of $\varepsilon = 3.5E5N/m$ is adopted as in [2]. However, in all beam-to-beam contact simulations a normal parameter of $\varepsilon = 1.5E6N/m$ is adopted. All simulations are dynamically performed with Newmark parameters $\beta = 0.3$ and $\gamma = 0.5$ [21]. A boundary condition with fixed displacements and free rotation is assumed at the end points of all yarns.

Experimental and modeling results for $k = 1$, $k = 2$, and $k = 0.5$ are presented in Figure 3. In this figure, the experimental results indicated as "Experimental" are adapted from [1], the surface-to-surface model results

indicated as ”Surface” are adapted from [2], and the beam-to-beam model results are calculated and indicated as ”Spline”. The results from Figure 3a show very similar responses between the ”Surface” and ”Spline” models. These results are, however, slightly “delayed” when compared to the experimental. This behavior is a side effect triggered by the out-of-plane spacing as observed in [2].

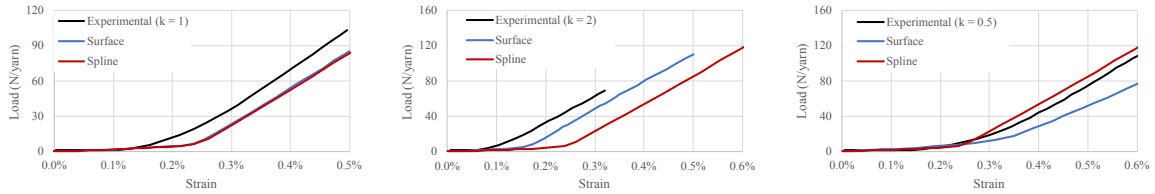

(a) $k = 1$. (b) $k = 2$. (c) $k = 0.5$.

Figure 3. Biaxial tension results, ”Experimental” in black from [1], ”Surface” in blue from [2], and ”Spline” in red from the spline-based contact formulation.

The results for $k = 2$ and $k = 0.5$ are respectively presented in Figures 3b and 3c. These figures show quite distinct mechanical behaviors from the “Surface” and the “Spline” models. By analyzing these models it was possible to observe that these differences are caused by the contact elements definition. In the “Spline” formulation the contact elements are defined according to a C^1 curve that is not interpolatory to the structural nodes. In the “Surface” formulation, however, the contact elements centroid is defined exactly as the beam axis. The mechanical response of the “Spline” model is, however, qualitatively similar to the experimental results from [1].

The normal contact forces from the “Spline” model and the “Surfaces” model [2] are presented in Figure 4. These figures show less normal contact forces with higher magnitude in the “Spline” model when compared to the “Surfaces” model. These results highlight two important modeling differences. The first difference is in the cross-sections used for defining the contact elements. In the “Spline” formulation circular cross-sections are adopted while in the “Surface” formulation elliptical cross-sections are considered. This difference leads to single forces at the contact regions as observed in 4b. The second difference is in the normal penalties adopted. In the “Spline” model a higher normal penalty is assumed when compared to the “Surface” model. The difference in the normal penalties is necessary since some multiple contacts are reduced to single-contact interactions. Moreover, the existence of single-contact interactions can be advantageous to implement experimentally-based interface laws.

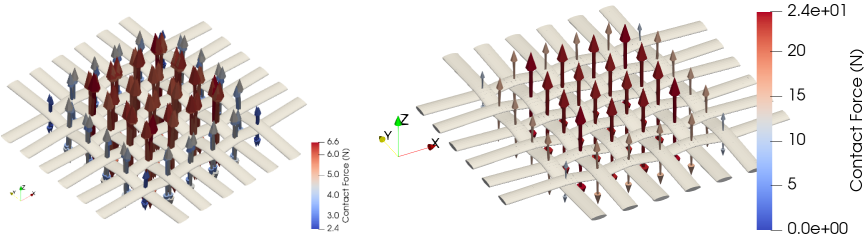

(a) Surface-to-surface contact formulation. Extracted from [2].

(b) Spline-based contact formulation.

Figure 4. Normal contact forces obtained from the biaxial modeling of a glass fabric plain weave for $k = 1$.

6 Conclusions

This work showed that it is possible to model the textiles’ mechanical behavior under biaxial tension by combining a structural beam theory and a contact formulation. The surface-to-surface and the beam-to-beam contact formulations were able to reproduce the plain weave glass fabric mechanical response qualitatively. The single-contact interaction pattern observed in the beam-to-beam formulation can be seen as an advantage to implementing experimentally-based interface laws.

Acknowledgements. The authors would like to acknowledge the National Council for Scientific and Technological Development (CNPq) under the grants 168927/2018-7 and 304321/2021-4, and the São Paulo Research Foundation (FAPESP) under the grant 2020/13362-1.

Authorship statement. The authors hereby confirm that they are the sole liable persons responsible for the authorship of this work, and that all material that has been herein included as part of the present paper is either the property (and authorship) of the authors, or has the permission of the owners to be included here.

References

[1] K. Buet-Gautier and P. Boisse. Experimental analysis and modeling of biaxial mechanical behavior of woven composite reinforcements. *Experimental Mechanics*, vol. 41, n. 3, pp. 260–269, 2001.
[2] C. J. Faccio Júnior and A. Gay Neto. Challenges in representing the biaxial mechanical behavior of woven fabrics modeled by beam finite elements with contact. *Composite Structures*, vol. 257, pp. 113330, 2021.
[3] C. J. Faccio Júnior, A. Gay Neto, and P. Wriggers. Spline-based smooth beam-to-beam contact model. *Computational Mechanics*, 2023.
[4] A. Konyukhov and K. Schweizerhof. Geometrically exact covariant approach for contact between curves. *Computer Methods in Applied Mechanics and Engineering*, vol. 199, n. 37-40, pp. 2510–2531, 2010.
[5] C. Meier, W. A. Wall, and A. Popp. A unified approach for beam-to-beam contact. *Computer Methods in Applied Mechanics and Engineering*, vol. 315, pp. 972–1010, 2017.
[6] A. Gay Neto, P. M. Pimenta, and P. Wriggers. A master-surface to master-surface formulation for beam to beam contact. Part I: Frictionless interaction. *Computer Methods in Applied Mechanics and Engineering*, vol. 303, pp. 400–429, 2016.
[7] A. Gay Neto, P. M. Pimenta, and P. Wriggers. A master-surface to master-surface formulation for beam to beam contact. part ii: Frictional interaction. *Computer Methods in Applied Mechanics and Engineering*, vol. 319, pp. 146–174, 2017.
[8] C. J. Faccio Júnior, A. Gay Neto, and P. Wriggers. Numerical strategy for solving general C1 -continuous beam-to-beam contact problems (under review). *International Journal for Numerical Methods in Engineering*, 2024.
[9] A. Gay Neto and P. Wriggers. Numerical method for solution of pointwise contact between surfaces. *Computer Methods in Applied Mechanics and Engineering*, vol. 365, 2020.
[10] L. Piegl and W. Tiller. *The NURBS book*, volume 35 of *Monographs in Visual Communication*. Springer Berlin Heidelberg, Berlin, Heidelberg, 1997.
[11] J. C. Simo. A finite strain beam formulation. The three-dimensional dynamic problem. Part I. *Computer Methods in Applied Mechanics and Engineering*, vol. 49, n. 1, pp. 55–70, 1985.
[12] J. C. Simo and L. Vu-Quoc. A three-dimensional finite-strain rod model. part II: Computational aspects. *Computer Methods in Applied Mechanics and Engineering*, vol. 58, n. 1, pp. 79–116, 1986.
[13] J. C. Simo and L. Vu-Quoc. A Geometrically-exact rod model incorporating shear and torsion-warping deformation. *International Journal of Solids and Structures*, vol. 27, n. 3, pp. 371–393, 1991.
[14] P. M. Pimenta and T. Yojo. Geometrically exact analysis of spatial frames. *Applied Mechanics Reviews*, vol. 46, n. 11, pp. S118–S128, 1993.
[15] P. M. Pimenta and E. M. B. Campello. Geometrically nonlinear analysis of thin-walled space frames. In *Proceedings of the Second European Conference on Computational Mechanics, II ECCM*, 2001.
[16] T. Yojo. *Análise Não-Linear Geometricamente Exata de Pórticos Espaciais*. PhD thesis, 1993.
[17] A. Gay Neto. "Giraffe user's manual" - generic interface readily accessible for finite elements. pp. 1–70, 2020.
[18] A. G. Neto, C. A. Martins, and P. M. Pimenta. Static analysis of offshore risers with a geometrically-exact 3D beam model subjected to unilateral contact. *Computational Mechanics*, vol. 53, n. 1, pp. 125–145, 2014.
[19] A. Gay Neto. Dynamics of offshore risers using a geometrically-exact beam model with hydrodynamic loads and contact with the seabed. *Engineering Structures*, vol. 125, pp. 438–454, 2016.
[20] L. Brown and A. Long. Modeling the geometry of textile reinforcements for composites: TexGen. In *Composite Reinforcements for Optimum Performance*, pp. 237–265. Elsevier, 2021.
[21] A. Ibrahimbegović and S. Mamouri. On rigid components and joint constraints in nonlinear dynamics of flexible multibody systems employing 3D geometrically exact beam model. *Computer Methods in Applied Mechanics and Engineering*, vol. 188, n. 4, pp. 805–831, 2000.